

New Heart Features for More Effective Human Identification

<https://doi.org/10.3991/ijoe.v18i08.31317>

Safe S.I

Malaysian Institute of Industrial Technology, Universiti Kuala Lumpur, Johor, Malaysia
sairulizwan@unikl.edu.my

Abstract—Biometric verification is a process to authenticate whether the subject is what it claims to be, based on the characteristics of the human body. These characteristics must meet seven (7) conditions to enable them to be used in a practical biometric system. These conditions are namely distinctiveness, performance, collectability, acceptability, universality, circumvention, and permanence. Electrocardiogram (ECG) is a human body characteristic measured from the heart that meets these seven conditions. Choosing the correct features from the ECG is important to get a high authentication rate. This paper proposed a new algorithm known as Bipolar Slope Feature (BSF) for ECG features selection. It is developed based on the relationship of slopes between several locations in a complete ECG cycle. The Receiver Operating Characteristic (ROC) curve is used to measure the effectiveness of this technique for the application of biometric verification.

Keywords—authentication, biometric, human identification, electrocardiogram, feature extraction

1 Introduction

A biometric system is a system that compares certain characteristics of a person, for recognition. It operates either in authentication or identification mode [1]. In authentication mode, first, the user will claim an identity stored in the database. The stored data is in the form of feature vectors. Next, the user will submit their respective biometric traits for feature vectors extraction. Both features (stored and newly submitted) are then compared to ensure that the claimed identity is valid [2]. As for the identification mode, the newly submitted feature vectors is compared to all feature vectors stored in the system. Feature vectors with the highest similarity determines the identity of the user [3].

Human body biometric features can be classified into external body, behavioral and internal body characteristics. Examples of external body characteristic are fingerprints [4], iris and facial [5], while examples of behavioral traits are voice [6] and signature [7]. Electrocardiogram (ECG) and electroencephalogram (EEG) are two examples of internal body features [8].

Recently, ECG has been the choice of researchers, for practical use in a biometric system. The characteristics of the human body must meet 7 conditions before it can be

used as the official feature for a practical biometric system [1]. First, it must be universal which means, this feature must be possessed by everyone. An ECG is a signal produced by heart. Since all living human beings must have a heart, ECG has met the first requirements to be considered as a feature for a practical biometric system.

ECG meets the second requirement to be practically considered as biometric features, which is the distinctiveness. It means that the ECGs are different between individuals. Studies conducted in [9] prove that the distinctiveness of ECG are influenced by factors such as gender [10], age, blood mass-torso, torso-air conductivity [11], body shape, geometric shape of the heart and race [12].

The ECG is also invariant for a period of time [13, 14], which is the third criteria to be considered as biometric features. Furthermore, ECG can be measured quantitatively using the electrocardiograph machines, which is the fourth criteria [15]. The fifth, sixth and seventh criteria are circumvention, acceptability and performance [16]. The use of ECG as a feature in biometric systems is also difficult to be deceive. Since ECG signals are generated by the heart, it is impossible for scammers to accurately duplicate user ECG signals [17]. The ECG also have a similar problem faced by other biometric features, namely protecting the user privacy. ECG stores a large amount of health information for a subject. This information is sensitive to users and may not be shared without permission [18]. By ensuring that this information is not leaked, ECG has the potential to be used as a biometric feature. In terms of performance, ECG biometric system yields at least 80% of positive classification rate [19, 20, 21].

ECG represents the electrical activity generated from the heart. Its morphology is shown in Figure 1. As can be seen in Figure 1, a complete ECG cycle measured from a healthy individual, has 3 main waves namely P, QRS and T. Each of these waves has peaks and boundaries. Information such as amplitude, duration and slope measured between these points are usually selected as biometric features [22, 23].

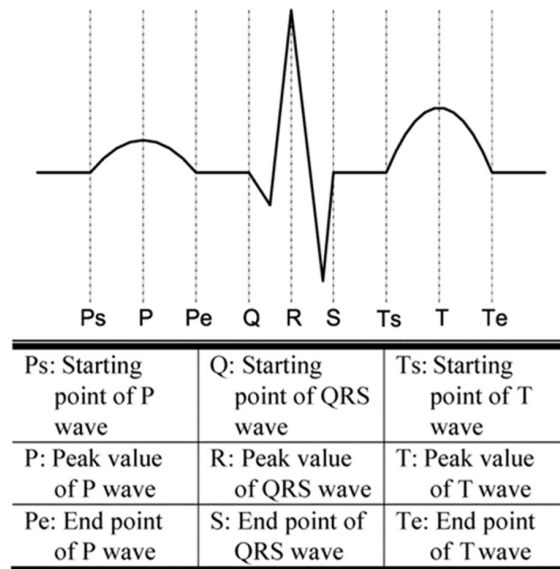


Fig. 1. Typical ECG morphology

2 Objective

Features based on the slope of the pulse domain techniques have been introduced in [24]. In this paper, an extended version of the slope feature is presented. In [24], a slope feature equation is constructed based on the concept of superimposing a single triangular wave with the ECG signals. In this paper, two periodic triangular wave with an opposite polarity is used to construct a new equation of a slope feature.

Be as it may, processing ECG signals for biometric purposes need to deal with 2 issues, amplitude and heart rate variabilities. These two issues usually affects the recognition rate of a person [24, 25].

This paper focuses on overcoming these two problems. The outline of this paper begins by explaining the development of new feature techniques based on the slope of the pulse domain features in section 2. It is followed by the discussion on experimental setup and the performance results of the new proposed features, respectively in sections 3 and 4 before section 5 concludes this paper.

3 Research method

3.1 Bipolar pulse active slope

Features based on the slope of the pulse domain techniques have been introduced in [24]. In this paper, an extended version of the slope feature is presented. In [24], a slope feature equation is constructed based on the concept of superimposing a single triangular wave with the ECG signals. In this paper, two periodic triangular wave with an opposite polarity is used to construct a new equation of a slope feature.

Figure 2 illustrates an ECG signal, $y_{ECG}(t)$ from the peak of P to the peak of T . The duration between these two peaks is T_{ECG} . $y_{ECG}(t)$ has a peak-to-peak amplitude of A_{ECG} and requires to be offset until its minimum value is zero. Two periodic triangular waves, $y_{Tri_1}(t)$ and $y_{Tri_2}(t)$, is first generated to be superimposed on $y_{ECG}(t)$ [26]. The duration and peak-to-peak amplitude, for both triangular waves are T_{Tri} and A_{Tri} respectively.

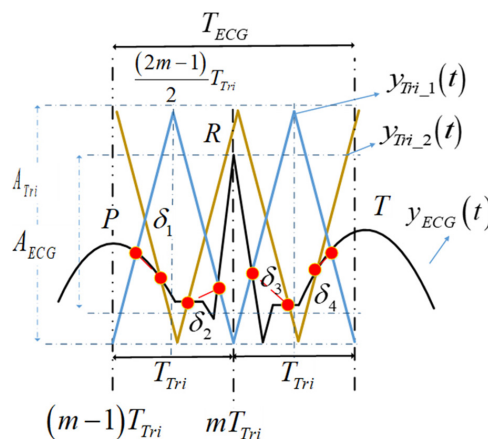


Fig. 2. Bipolar pulse active technique

According to [13], the relationship between $y_{ECG}(t)$ and a triangular wave can be define as integer modulation factor, m_f and modulation index, m_i and can mathematically formulated as:

$$m_f = \frac{T_{ECG}}{T_{Tri}} \quad (1)$$

$$m_i = \frac{A_{Tri}}{A_{ECG}} \quad (2)$$

In general, for $t = t_{A(2m-1)}$ between $(m-1)T_{Tri}$ and $\frac{(2m-1)}{2}T_{Tri}$, let y_b and y_a represent the maximum and minimum point of the triangular wave $y_{Tri_1}(t)$ respectively. Let x_a and x_b represent the starting and ending sampling points and let y_c and x_c represent the coordinate which the triangular wave intersects with y-axis, respectively. The positive slope for $y_{Tri_1}(t)$ can be mathematically described as:

$$y_{Tri_1}(t) = \frac{2(y_b - y_a)(t_{A(2m-1)} - x_c) + (T_{Tri} - 2)y_c}{T_{Tri} - 2} \quad (3)$$

By shifting $y_{Tri_1}(t)$ so that its minimum value equal to zero (i.e $y_a = 0$), we then normalizing the peak amplitude of $y_{ECG}(t)$ to 1. By doing so, $y_b = m_i$ and equation (3) become:

$$y_{Tri_1}(t) = \frac{2m_i(t_{A(2m-1)} - x_c) + (T_{Tri} - 2)y_c}{T_{Tri} - 2} \quad (4)$$

From Figure 1, it is observed that $x_c = x_a$ and $y_c = y_a$. Substituting equation (1) into (4) yields:

$$y_{Tri_1}(t) = -\frac{2m_i(m_f(1-t_{A(2m-1)}) + T_{ECG}(m-1))}{T_{ECG} - 2m_f} \quad (5)$$

The negative slope of $y_{Tri_2}(t)$ can be obtained for $t = t_{B(2m-1)}$ between $(m-1)T_{Tri}$ and $\frac{(2m-1)}{2}T_{Tri}$ by reversing the polarity of (5) as follows:

$$y_{Tri_2}(t) = \frac{2m_i(m_f(1-t_{B(2m-1)}) + T_{ECG}(m-1))}{T_{ECG} - 2m_f} \quad (6)$$

In equations (5) and (6), $m = 1, 2, 3 \dots m_f$. $t_{A(2m-1)}$ and $t_{B(2m-1)}$ represent respectively the first intersection points for $y_{Tri_1}(t)$ and $y_{Tri_2}(t)$ intersecting the underlying ECG signal.

The slope, δ_{2m-1} of $t_{A(2m-1)}$ and $t_{B(2m-1)}$ between $(m-1)T_{Tri}$ and $\frac{(2m-1)}{2}T_{Tri}$ is taken as features. This can be computed as follow:

$$\delta_{(2m-1)} = \frac{2(2(m-1)T_{ECG} - (t_{A(2m-1)} + t_{B(2m-1)} - 2)m_f)m_i}{(-T_{ECG} + 2m_f)(t_{A(2m-1)} - t_{B(2m-1)})} \quad (7)$$

for $m = 1, 2, 3, \dots, m_f$.

Similar procedure is performed from equations (3) to (6) to generate a general representation of $y_{Tri_1}(t)$ and $y_{Tri_2}(t)$ for $t = t_{A(2m)}$ and $t = t_{B(2m)}$ between $\frac{(2m-1)}{2}T_{Tri}$ and mT_{Tri} respectively as follows:

$$y_{Tri_1}(t) = \frac{2m_i(-m_f t_{A(2m)} + T_{ECG} m)}{T_{ECG}} \quad (8)$$

$$y_{Tri_2}(t) = \frac{2m_i(m_f t_{B(2m)} - T_{ECG} m)}{T_{ECG}} \quad (9)$$

The value of m in equations (7) and (8) is also equal to $1, 2, 3, \dots, m_f$. Thus, the slope, δ_{2m} of $t_{A(2m)}$ and $t_{B(2m)}$ between $\frac{(2m-1)}{2}T_{Tri}$ and mT_{Tri} is then taken as features and can be calculated as:

$$\delta_{2m} = \frac{2m_i(2mT_{ECG} - (t_{A(2m)} + t_{B(2m)})m_f)}{T_{ECG}(t_{A(2m)} - t_{B(2m)})} \quad (10)$$

3.2 Simulation setup

ECG lead refers to the tracing of the voltage between two points on the human body. It consists of two electrodes of opposite polarity or one electrode, and a reference point made up from a signal combination of other electrodes [27].

ECG was recorded from the fingers of both hands of our subjects. This recording method is referred to as lead-1 ECG configuration recording. It is the most practical ECG recording method for biometric applications [28]. MD100E handheld ECG machine as shown in Figure 3 is used to record the ECG signal in our study. A standard ECG signals recording using MD100E last for 30 seconds with sampling frequency of 250 Hz.



Fig. 3. MD100E Handheld ECG recording process

To test the effectiveness of the proposed technique, we have recorded 1000 ECG recordings from 100 participants in developing the test and training databases. Each participant submitted 10 ECG recordings per week for these databases. The process of generating these databases is shown in Figure 4.

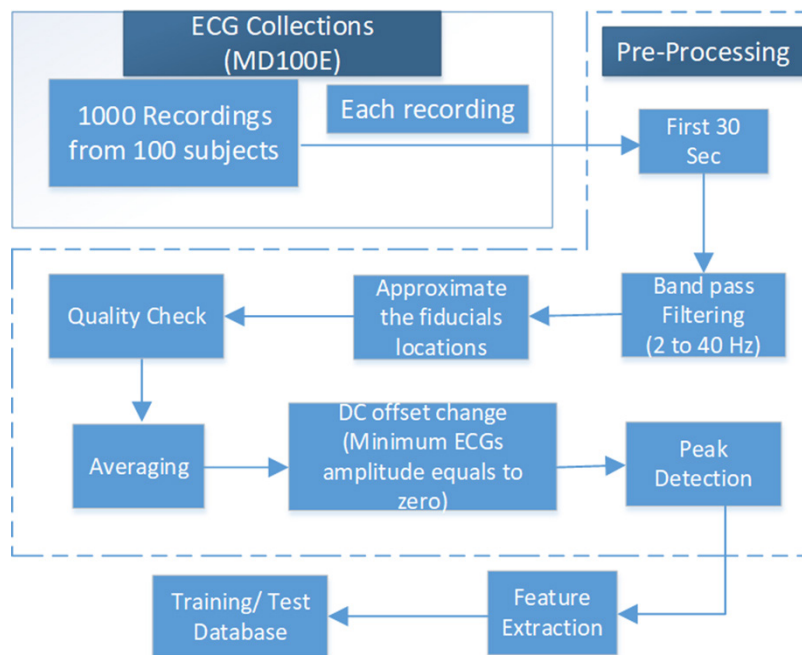


Fig. 4. Summary of setting up simulation setup

For every 30 seconds of the ECG recording, a quality inspection process will be performed on the signal. This is to ensure, only a complete and clear ECG cycles can be used for further process. A complete and clear ECG cycle we define as an ECG cycle that has a clear and complete morphology of P, QRS and T waves. The peaks of R for these quality ECG waves are then detected, aligned to this peak and averaged.

The minimum value of this average ECG is offset by its DC value until the minimum value is zero. Then, the P and R peaks of this average signal are again detected, segmented before its unique features are extracted. These features are then set as the training or test databases.

The performance of the extracted features will be measured using two parameters, namely the Receiver Operating Characteristic (ROC) curves and Normalized Euclidean Distance score, $|\text{Score}_{\text{ED}}|$ [29]. Mathematically it can be explained as follows:

$$|\text{Score}_{\text{ED}}| = 1 - \frac{\text{Score}_{\text{ED}}}{\text{Score}_{\text{maxED}}} \quad (11)$$

where Score_{ED} is the Euclidean Distance between the test and training features. $\text{Score}_{\text{maxED}}$ on the other hand, is the maximum Euclidean Distance for all features in the test and training databases.

4 Results and discussion

The proposed feature presented as in equation (7) and (10) are dependable to user defined values of m_j and m_i . In this section, example of generating the BSF is first discussed. It follows by the discussion on generating the ROC curves. Finally, the effect of changing the values of m_j and m_i is then explained.

4.1 Numerical example of bipolar slope feature

To illustrate the example of generating the BSF, we defined m_j and m_i as 2 and 1.5. The location of T_{ECG} is selected from the peak of P to the peak of T. Using this setting, $y_{\text{Tri}_1}(t)$ and $y_{\text{Tri}_2}(t)$ are generated and superimposed on $y_{\text{ECG}}(t)$ as shown in Figure 5.

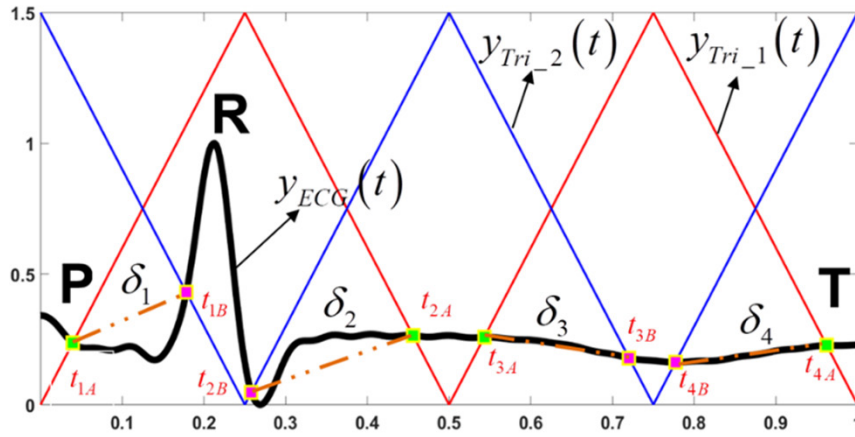


Fig. 5. Example of δ_m features for ECG trace between P and T with $m_f = 2$ and $m_i = 1.5$

The intersection location between these signals and the calculated value of the BSF from equations (7) and (10) is given in Table 1.

Table 1. Example of the intersection locations and the calculated BSF for Figure 5

	$m = 1$	$m = 2$
$t_{(2m-1)A}$	0.0392	0.5430
$t_{(2m-1)B}$	0.1784	0.7230
$\delta_{(2m-1)}$	1.3966	1.0968
$t_{(2m)A}$	0.4559	0.9622
$t_{(2m)B}$	0.2580	0.7769
$\delta_{(2m)}$	-0.4505	0.3522

4.2 Generating ROC curves

In this subsection, a step-by-step example is shown, to produce the ROC curve. In this example, BSF is extracted from four different subjects, namely S1, S2, S3 and S4 as in Table 2. In this example, all subjects send their ECG twice. The first ECG is to create a training database, while the second ECG is for the test database. We still use $m_f = 2$ and $m_i = 1.2$ in this example.

The feature vector for all subjects in the training database will be compared to all subjects in the test database, to generate $SCORE_{ED}$. In this example, Normalize Euclidean Distance as in (11) is used as similarity measures. In our database, $SCORE_{maxED}$ is calculated as 25.775. Table 3 compares the $|SCORE_{ED}|$ of equation (11) for all 4 subjects.

As can be observed from Table 3, if the subjects from the training and test databases are the same, they produce a positive authentication (+) in the column AA. Otherwise; they generate negative authentication (-). There should be only 4 positive authentications and only 12 negative authentications for this example, as presented in Table 3.

Table 2. Example of BSF from 4 different subject

	Training			
	δ_1	δ_2	δ_3	δ_4
S1	-0.413	-6.267	0.027	1.109
S2	-0.404	-4.965	-0.115	0.262
S3	1.126	1.199	-0.462	0.373
S4	-1.325	-3.733	1.158	0.454
	Test			
	δ_1	δ_2	δ_3	δ_4
S1	-0.226	-5.455	0.036	0.844
S2	-0.412	-4.813	-0.827	0.244
S3	0.985	1.179	-0.430	0.395
S4	-1.550	-4.883	1.133	0.309

The ROC curve is generated based on the selection of all thresholds in the system. These threshold values will be compared with $|SCORE_{ED}|$ in Table 3. The selected threshold values are between 0 and 1. In this paper, we only show the predicted authentication result for 3 threshold values (ThA), namely 0.75, 0.85 and 0.95, as shown in Table 4.

Table 3. Example of $|SCORE_{ED}|$ as in (11) from 4 subjects

Train	Test	$ SCORE_{ED} $	AA
S1	S1	0.966	+
	S2	0.926	-
	S3	0.704	-
	S4	0.913	-
S3	S1	0.735	-
	S2	0.759	-
	S3	0.994	+
	S4	0.735	-
S2	S1	0.969	-
	S2	0.972	+
	S3	0.755	-
	S4	0.934	-
S4	S1	0.9083	-
	S2	0.9051	-
	S3	0.7806	-
	S4	0.9492	+

Note: AA defined as either actual positive authentication (+) or actual negative authentication (-) results.

To facilitate this discussion, let’s examine the predicted authentication results, shown in the third column of Table 4, for threshold value (ThA) set at 0.75. The predicted authentication is made after the $|SCORE_{ED}|$ value is compared with the ThA value.

Table 4. Prediction authentication based on threshold value equals to 0.2, 0.4 and 0.8

AA	$ SCORE_{ED} $	ThA 0.75	ThA 0.85	ThA 0.95
+	0.966	+	+	+
-	0.926	+	+	-
-	0.704	-	-	-
-	0.913	+	+	-
-	0.735	-	-	-
-	0.759	+	-	-
+	0.994	+	+	+
-	0.735	-	-	-
-	0.969	+	+	+
+	0.972	+	+	+
-	0.755	+	-	-
-	0.934	+	+	-
-	0.9083	+	+	-
-	0.9051	+	+	-
-	0.7806	+	-	-
+	0.9492	+	+	-

If $|SCORE_{ED}|$ is greater than ThA, the system predicts that it is a positive authentication. Similarly, if $|SCORE_{ED}|$ is less than the ThA value, the system will predict it is a negative authentication. In the third column, there are 13 positive authentications and 4 negative authentications. The summary of the predicted authentication for all three ThA values is shown in Table 5. For ThAs set to 0.85 and 0.95, the predicted positive authentications are 10 and 5 while the predicted negative authentications are 6 and 11.

Let’s observe at the prediction results for $|SCORE_{ED}|$ equal to 0.926 (in the second row of Table 4). Since $|SCORE_{ED}|$ is greater than the ThA values set to 0.75 and 0.85, the system predicts that both results are authenticated as a positive authentication. In actual fact, the system should predict a negative authentication. The wrongly classify predicted positive authentication results based on these two ThA values, is defined as ‘False Acceptance’ (FA).

Still in the same row, we can see that the value of $|SCORE_{ED}|$ is less than ThA value. Therefore, the system has predicted it as a negative confirmation. Since both real and predicted authentication is negative, this condition is defined as ‘True Rejection’ (TR). Let’s see another example, for $|SCORE_{ED}|$ equal to 0.9492 (in the last row of Table 4). The system predicted a positive authentication for ThAs set to 0.75 and 0.85. Since the actual and predicted authentication is positive, the system is said to generate a ‘True

Acceptance (TA)’ condition for these ThAs. However, for ThA set to 0.95, the ThA value is greater than $|SCORE_{ED}|$, hence the system predicted it as a negative authentication. This misclassification result (between actual and prediction) is defined as ‘False Rejection (FR)’. The comparison between actual and predicted authentication is given in Table 5.

Table 5. Calculation of True Acceptance Rate (TAR) and False Acceptance Rate (FAR)

Threshold	Total		Total		TAR	FAR
	AA(+)	AA(-)	TA	FA		
0.75	4	12	4	9	1	0.75
0.85	4	12	4	6	1	0.50
0.95	4	12	3	1	0.75	0.08

The ROC curve plot, is a function of the decision threshold, which plots the rate of ‘False Acceptance (FAR)’ (i.e. impostor accepted as genuine) on the x-axis, against ‘True Acceptance Rate (TAR)’ (i.e. genuine accepted as genuine) on the y-axis. TAR and FAR in Table 5 can be calculated as follows:

$$TAR = \frac{\text{True Acceptance}}{\text{Actual Number of Positive Authentication}} \quad (12)$$

$$FAR = \frac{\text{False Acceptance}}{\text{Actual Number of Negative Authentication}} \quad (13)$$

FAR will be plotted against TAR for all ThA values to generate the ROC curves. Using more threshold values and number of subjects, a smoother ROC curve can be obtained as illustrated in Figure 6.

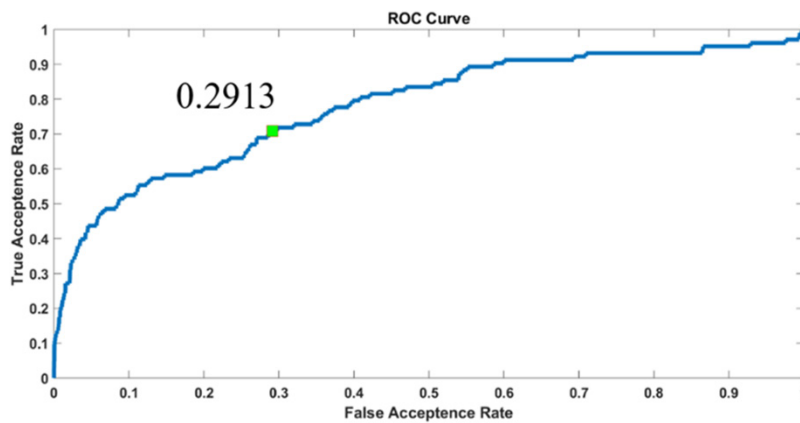


Fig. 6. Example of ROC curves

5 Discussion

In order to quantitatively measure the comparison of multiple ROC curve performances, the area under an ROC (AUR) and the Equal Error Rate (ERR) are used. The AUR calculates the area under each of the ROC curve. Its value ranges between 0 and 1. The AUR has an important statistical property which is equivalent to an average of the overall performance of the biometric system when all threshold settings generating the ROC curves are considered. The EER is defined as the rate at which the FAR equals the 1-TAR. EER ranges between 0 and 1. A higher AUR value with a lower value of EER is desirable for practical systems. For the example shown in Figure 6, it is shown that the EER for the ROC curves is equal to 0.2913.

Equations (7) and (10) are closely related to m_f and m_i values. To evaluate the effectiveness of selecting these values, in the next experiment, m_i is set between 0.6 and 2 while m_f is set between 1 and 10. Figure 8 illustrates the performance of EER based on these ranges. It can be seen from Figure 7 that lower EER is obtained by selecting m_f value of less than 2. It is also observed from Figure 7, the value of m_i does not have much effect on the EER value.

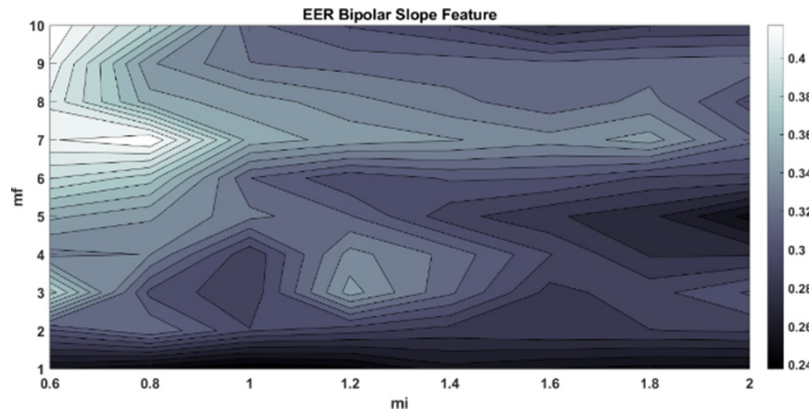


Fig. 7. EER performance

AUR performance when various values of m_f and m_i are used in equations (7) and (10) is shown in Figure 8. It is shown in this experiment that the AUC is higher when m_f is set to less than 2. This figure also shows that when m_i is set between 1 and 1.5, better authentication result can be obtained. From these two experiments, we can conclude that, the proposed BSF algorithm as in (7) and (10) should used m_f value that is less than 2 while m_i should be set between 1 and 1.5.

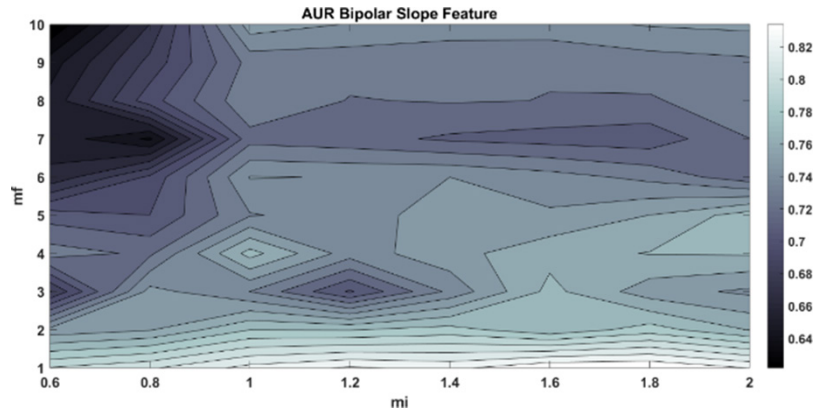


Fig. 8. AUR performance

6 Conclusion

This paper describes the development of novel algorithms known as the Bipolar Slope Feature (BSF), which is then used to extract the unique features of Electrocardiogram (ECG), for biometric authentication purposes. ECG is a recorded signal from the heart. BSF requires information such as the starting and ending points of the ECG signal, the modulation index (m_i) and the modulation factor (m_f), which determined by the user. In this work, the ECG is segmented between P and T peaks. The effects of using m_i values from 0.6 to 2 and m_f between 1 and 10 have been studied in this paper. 100 participants were used to produce the training and test databases. The calculated BSF features using various m_f and m_i settings, have been used to generate the Receiver Operating Characteristic (ROC) curves. Based on the analysis of the ROC curves, it is shown that better authentication performance is obtained for m_f less than 2 and m_i between 1 and 1.5.

7 References

- [1] A. K. Jain, A. Ross and S. Prabhakar, "An introduction to biometric recognition," *IEEE Transactions on Circuits and Systems for Video Technology*, vol. 14, no. 1, pp. 4–20, January 2004. <https://doi.org/10.1109/TCSVT.2003.818349>
- [2] N. D. Sarier, "Multimodal biometric authentication for mobile edge computing," *Information Sciences*, vol. 573, pp. 82–99, 2021. <https://doi.org/10.1016/j.ins.2021.05.036>
- [3] A. Jain, L. Hong and S. Pankanti, "Biometric identification," *Communications of the ACM*, no. 2, pp. 90–98, February 2000. <https://doi.org/10.1145/328236.328110>
- [4] D. Valdes-Ramirez, M. A. Medina-Pérez, R. Monroy, O. Loyola-González, J. Rodríguez, A. Morales and F. Herrera, "A review of fingerprint feature representations and their applications for latent fingerprint identification: Trends and evaluation," *IEEE Access*, vol. 7, pp. 48484–48499, 2019. <https://doi.org/10.1109/ACCESS.2019.2909497>

- [5] R. Coelho Dalapicola, R. Tavares Vieira Queiroga, C. Toledo Ferraz, T. Trevisan Negri Borges, J. Hiroki Saito and A. Gonzaga, “Impact of Facial Expressions on the Accuracy of a CNN Performing Periocular Recognition,” in *2019 8th Brazilian Conference on Intelligent Systems (BRACIS)*, 2019. <https://doi.org/10.1109/BRACIS.2019.00077>
- [6] R. Khanna, D. Oh and Y. Kim, “Through-wall remote human voice recognition using doppler radar with transfer learning,” *IEEE Sensors Journal*, vol. 19, no. 12, pp. 4571–4576, 2019. <https://doi.org/10.1109/JSEN.2019.2901271>
- [7] X. Shan, L. You and G. Hu, “Two efficient constructions for biometric-based signature in identity-based setting using bilinear pairings,” *IEEE Access*, vol. 9, pp. 25973–25983, 2021. <https://doi.org/10.1109/ACCESS.2021.3057064>
- [8] M. Wang, J. Hu and H. A. Abbass, “BrainPrint: EEG biometric identification based on analyzing brain connectivity graphs,” *Pattern Recognition*, p. 107381, 2020. <https://doi.org/10.1016/j.patcog.2020.107381>
- [9] A. v. Oosterom, R. Hoekema and G. Uijen, “Geometrical factors affecting the interindividual variability of the ECG and the VCG,” *Journal of electrocardiology*, vol. 33, pp. 219–227, 2000. <https://doi.org/10.1054/jelc.2000.20356>
- [10] L. S. Green, R. L. Lux, C. W. Haws, R. R. Williams, S. C. Hunt and M. J. Burgess, “Effects of age, sex and body habitus on QRS and ST-T potential maps of 1100 normal subjects,” *Circulation*, vol. 77, pp. 244–253, 1985. <https://doi.org/10.1161/01.CIR.71.2.244>
- [11] T. C. Pilkington, R. C. Barr and C. L. Rogers, “Effect of conductivity interfaces in electrocardiography,” *Bulletin of Mathematical Biology*, vol. 30, no. 4, pp. 637–643, 1968. <https://doi.org/10.1007/BF02476680>
- [12] D. N. Masica, B. J. Maron and L. Krovetz, “Racial variations in the childhood electrocardiogram: Preliminary observations,” *American Heart Journal*, vol. 84, no. 2, p. 153, 1972. [https://doi.org/10.1016/0002-8703\(72\)90329-8](https://doi.org/10.1016/0002-8703(72)90329-8)
- [13] Y. Wang, F. Agrafioti, D. Hatzinakos and K. N. Plataniotis, “Analysis of human electrocardiogram for biometric recognition,” *EURASIP Journal on Advances in Signal Processing*, vol. 2008, no. 148658, pp. 1–11, 2008. <https://doi.org/10.1155/2008/148658>
- [14] G. Wuebbeler, R. Boussejot and D. Kreiseler, “Human verification by heart beat signals,” Physikalisch-Technische Bundesanstalt (PTB), Berlin, 2004.
- [15] K.-K. Tseng, L. Fu, L. Liu, D. Lee, C. Wang, L. Li and Y. Meng, “Human identification with electrocardiogram,” *Enterprise Information Systems*, vol. 12, no. 7, pp. 798–819, 2018. <https://doi.org/10.1080/17517575.2018.1450526>
- [16] A. J. Bidgoly, Z. Arezoumand and H. J. Bidgoly, “A survey on methods and challenges in EEG based authentication,” *Computers & Security*, vol. 93, p. 101788, 2020. <https://doi.org/10.1016/j.cose.2020.101788>
- [17] T. Repcik, V. Polakova, V. Waloszek, M. Nohel, L. Smital, M. Vitek and R. Kolar, “Biometric authentication using the unique characteristics of the ECG signal,” *Computing in Cardiology*, pp. 1–4, 2020. <https://doi.org/10.22489/CinC.2020.321>
- [18] A. Ibaida, A. Abuadba and N. Chilamkurti, “Privacy-preserving compression model for efficient IoMT ECG sharing,” *Computer Communications*, vol. 166, pp. 1–8, 2921. <https://doi.org/10.1016/j.comcom.2020.11.010>
- [19] Y. Li, Y. Pang, K. Wang and X. Li, “Toward improving ECG biometric identification using cascaded convolutional neural networks,” *Neurocomputing*, vol. 391, pp. 83–95, 2020. <https://doi.org/10.1016/j.neucom.2020.01.019>
- [20] S.-K. Kim, C. Y. Yeun and P. D. Yoo, “An enhanced machine learning-based biometric authentication system using RR-interval framed electrocardiograms,” *IEEE Access*, vol. 7, pp. 168669–168674, 2019. <https://doi.org/10.1109/ACCESS.2019.2954576>
- [21] O. Chutatape, “A basic platform for the study of a wireless health telemonitoring system,” *Journal of Current Science and Technology*, pp. 69–77, 2011.

- [22] L. Biel, O. Pettersson, L. Philipson and P. Wide, “ECG analysis: a new approach in human identification,” *IEEE Transactions on Instrumentation and Measurement*, vol. 50, no. 3, pp. 808–812, 2001. <https://doi.org/10.1109/19.930458>
- [23] S. A. Israel, J. M. Irvine, A. Cheng, M. D. Wiederhold and B. K. Wiederhold, “ECG to identify individuals,” *Pattern Recognition*, vol. 38, no. 1, p. 133–142, 2004. <https://doi.org/10.1016/j.patcog.2004.05.014>
- [24] S. I. Safie, “ECG slope features for biometric authentication,” in *International Conference on Smart Instrumentation, Measurement and Application 2018 (ICSIMA)*, Songkhla, Thailand, 2018. <https://doi.org/10.1109/ICSIMA.2018.8688793>
- [25] S. I. Safie, J. J. Soraghan and L. Petropoulakis, “Electrocardiogram (ECG) biometric authentication using pulse active ratio (PAR),” *IEEE Transactions on Information Forensics and Security*, vol. 6, no. 4, pp. 1315–1322, December 2011. <https://doi.org/10.1109/TIFS.2011.2162408>
- [26] S. I. Safie, H. Nurfazira, Z. Azavitra, J. J. Soraghan and L. Petropoulakis, “Pulse Active Transform (PAT): A non-invertible transformation with application to ECG biometric authentication,” in *2014 IEEE REGION 10 SYMPOSIUM*, 2014. <https://doi.org/10.1109/TENCONSpring.2014.6863117>
- [27] M. Ingale, R. Cordeiro, S. Thentu, Y. Park and N. Karimian, “ECG biometric authentication: A comparative analysis,” *IEEE Access*, vol. 8, pp. 117853–117866, 2020. <https://doi.org/10.1109/ACCESS.2020.3004464>
- [28] M. N. Sahadat, E. L. Jacobs and B. I. Morshed, “Hardware-efficient robust biometric identification from 0.58 second template and 12 features of limb (Lead I) ECG signal using logistic regression classifier,” in *36th Annual International Conference of the IEEE Engineering in Medicine and Biology Society*, 2014. <https://doi.org/10.1109/EMBC.2014.6943871>
- [29] M. B. Madson, J. W. Schutts, H. R. Jordan, M. C. Villarosa-Hurlocker, R. B. Whitley and R. S. Mohn, “Identifying at-risk college student drinkers with the AUDIT-US: A receiver operating characteristic curve analysis,” *Assessment*, pp. 1–10, 2018. <https://doi.org/10.1177/1073191118792091>

8 Author

Safie S.I., Universiti Kuala Lumpur, Malaysian Institute of Industrial Technology, Johor, Malaysia.

Article submitted 2022-03-24. Resubmitted 2022-04-23. Final acceptance 2022-04-24. Final version published as submitted by the authors.